Journal of Hazardous Materials 506 (2026) 141653

Contents lists available at ScienceDirect

Journal of Hazardous Materials

journal homepage: www.elsevier.com/locate/jhazmat

Comparative study of WO_3 and WS_2 nanoparticles in regulating antibiotic resistance gene transfer: Implications for differential roles of metal oxides and sulfides

Zongling Tang [a,b], Wenhai Liu [a,b], Chao Wang [a,b], Fan Wang [a,b], Jialin Shi [a,b], Wanjun Wang [a,b,*]

[a] Guangdong Key Laboratory of Environmental Catalysis and Health Risk Control, Guangdong Hong Kong-Macao Joint Laboratory for Contaminants Exposure and Health, Institute of Environmental Health and Pollution Control, Guangdong University of Technology, Guangzhou 510006, China
[b] Guangzhou Key Laboratory Environmental Catalysis and Pollution Control, Guangdong Basic Research Center of Excellence for Ecological Security and Green Development, School of Environmental Science and Engineering, Guangdong University of Technology, Guangzhou 510006, China

HIGHLIGHTS

- WO_3 NPs exhibited higher conjugative transfer frequencies of ARGs than WS_2 NPs.
- Deeper integration with cell membrane was found in WO_3 than WS_2-exposure group.
- WO_3 NPs also induced higher SOS response, energy metabolism, and cell adhesion.
- Differential expression of genes governing conjugative transfer behaviors was verified.
- MONPs exerted a potential similar higher promoting effect on HGT of ARGs than MSNPs.

GRAPHICAL ABSTRACT

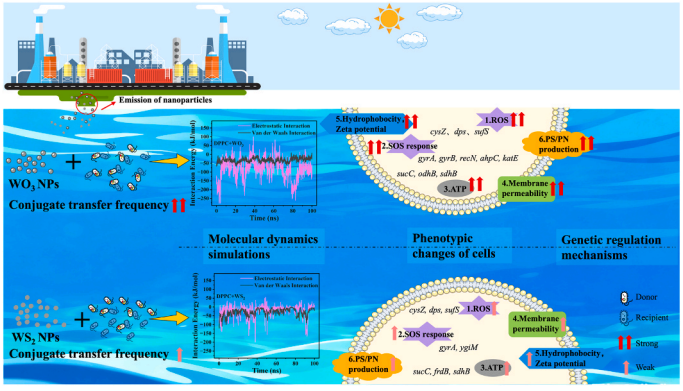

ARTICLE INFO

Keywords:
Antibiotic resistance genes
Metal oxide nanoparticles
Metal sulfide nanoparticles
Molecular dynamics simulation
Transcriptomic analysis

ABSTRACT

Non-antibiotic environmental stressors, such as nanoparticles, are emerging as potential drivers for regulating antibiotic resistance genes (ARGs) transmission via horizontal gene transfer. However, the differences between metal oxide nanoparticles (MONPs) and metal sulfide nanoparticles (MSNPs) in facilitating ARGs spread have not been explored. This study presented the first investigation into the divergent effects of WO_3 and WS_2 on plasmid-mediated conjugative transfer of ARGs. Results demonstrated that WO_3 and WS_2 significantly enhanced ARGs conjugative transfer at environmental-relevant concentrations (0.01–0.1 mg/L), with WO_3 showing a stronger promotion (up to 2.75-fold) than WS_2 (1.83-fold). WO_3 induced higher intracellular ROS and ATP levels than WS_2, and molecular dynamics simulations indicated a stronger binding affinity of WO_3 to lipid membranes, leading to increased membrane permeability. Zeta potential and cell surface hydrophobicity results indicated

* Corresponding author at: Guangdong Key Laboratory of Environmental Catalysis and Health Risk Control, Guangdong Hong Kong-Macao Joint Laboratory for Contaminants Exposure and Health, Institute of Environmental Health and Pollution Control, Guangdong University of Technology, Guangzhou 510006, China.
E-mail address: wanjun@gdut.edu.cn (W. Wang).

https://doi.org/10.1016/j.jhazmat.2026.141653
Received 8 November 2025; Received in revised form 21 January 2026; Accepted 28 February 2026
Available online 2 March 2026

that WO_3 stress exerted stronger intercellular adhesion compared with WS_2. Transcriptomic analysis consistently identified differential expression of genes associated with oxidative stress, energy metabolism, membrane integrity, and cell adhesion. Moreover, six additional MONPs and MSNPs were tested, consistently demonstrating that MONPs promote conjugative transfer of ARGs more efficiently than their MSNP counterparts. These results not only suggest that WO_3 exhibited higher risks than WS_2 in promoting ARGs dissemination, but also provide valuable insights into distinct roles of broad MONPs and MSNPs, potentially guiding the management of ARGs propagation while applying nanotechnology.

1. Introduction

One of the biggest threats to global public health is antibiotic resistance [1]. Worldwide, lakes, rivers, oceans, groundwater, rivers, oceans, and even drinking water have diverse antibiotic resistance genes (ARGs) [2]. Through conjugation, transduction, and transformation, horizontal gene transfer (HGT) has been reported to be responsible for disseminating ARGs in aquatic environments [3]. Among these, plasmid-mediated conjugative transfer is regarded as the most prevalent and requires particular attention [4]. Previous research has demonstrated that environmental pressures have a substantial impact on the spread of ARGs. However, although traditional research has established the role of various antibiotics in promoting bacterial resistance, growing evidence indicates that HGT of ARGs is also modulated by various non-antibiotic stressors, including organic pollutants [5], heavy metals [6], disinfectants [7], antiseptic chemicals [8], and emerging contaminants like microplastics [9]. Therefore, for a comprehensive knowledge of ARGs' transmission, it is very important to elucidate the role of these non-antibiotic stresses in the transmission of ARGs in aquatic systems.

Engineered nanoparticles (ENPs), represented by metal oxide nanoparticles (MONPs) and metal sulfide nanoparticles (MSNPs), have been frequently found in a variety of aqueous environments and have been used as another non-antibiotic stressor hotspot for influencing ARGs' dissemination [10]. For instance, among MONPs, ZnO and Al_2O_3 NPs significantly increased conjugative transfer (by 24.3-fold and 200-fold, respectively) by modulating membrane permeability [11,12]. Meanwhile, CuO NPs increased interspecific conjugative transfer by 4-fold, with excessive ROS production being identified as a major contributor [13]. Among MSNPs, by activating robust bacterial antioxidant systems, ZnS and sphalerite increased conjugative transfer by more than 10-fold compared to the control [14]. Xu et al., [15] conducted transcriptomic analysis which revealed that MoS_2 NPs upregulate amino acid metabolism genes, stimulating extracellular polymeric substance (EPS) secretion and increasing conjugative transfer frequency by 6.6-fold. However, these studies have primarily focused on individual ENPs, lacking a concurrent comparison of MONPs and MSNPs under consistent mechanistic frameworks.

Among typical MONPs and MSNPs, tungsten trioxide (WO_3) and tungsten disulfide (WS_2) have garnered increasing attention due to their broad applications as electrode materials [16], optical sensors [17], and functional materials in environmental remediation [18]. With the wide application of these materials, they have inevitably entered the aquatic environment and may exert impacts on the aquatic microbiome and resistome. Francis et al., [19] have reported that WO_3 NPs possessed antibacterial properties due to ROS-induced lipid peroxidation of bacterial cells. Meanwhile, WS_2 NPs was also found to affect bacterial viability via direct physical contact to disrupt membrane integrity [20]. There is a possible connection between the antibacterial properties of environmental stressors and the spread of ARGs. For example, the antibacterial properties of silver nanoparticles could promote plasmid-mediated conjugative transfer by 1.8-fold due to damage to cell membranes [21]. By analogy, it is speculated that WO_3 and WS_2 NPs may exert divergent effects on HGT in aquatic environments. However, the differential effects of WO_3 and WS_2 NPs on HGT of ARGs and the underlying molecular mechanisms are unknown.

To fill this research gap, WO_3 and WS_2 NPs were used as typical MONPs and MSNPs to investigate their differential effects on plasmid-mediated conjugative transfer of ARGs at environmentally relevant concentrations. Intracellular ROS levels, ATP regulation, EPS secretion, cell membrane permeability, bacterial surface hydrophobicity, and zeta potential were examined to determine the mechanisms governing conjugative transfer frequencies. Furthermore, to understand the mechanisms at both molecular and genetic levels, molecular dynamics simulations and RNA transcriptome sequencing were employed. Moreover, to explore potential broad trends in conjugative HGT of ARGs across MONPs and MSNPs, 6 additional representative MONPs (SnO_2, CuO, ZnO) and MSNPs (SnS_2, CuS, ZnS) were also evaluated for their effects on conjugative transfer. To the best of our knowledge, this is the first study to investigate the impacts of WO_3 and WS_2 NPs on conjugative HGT of ARGs and to systematically compare the differential roles of MONPs and MSNPs. While previous research has focused on how individual types of nanoparticles affect ARGs transfer, limited study has systematically compared oxide and sulfide nanoparticles of the same metal under uniform experimental conditions. The findings in this study not only clarify the environmental risks of WO_3 and WS_2 in promoting ARGs transmission, but also highlight the differences between MONPs and MSNPs in driving the spread of ARGs, thus providing potential guidance for environmental safety management of broad nanomaterials.

2. Materials and methods

2.1. Bacterial strains and other materials

The donor strain, *E. coli* DH5α, carries the RP4 plasmid that confers resistance to ampicillin, kanamycin, and tetracycline (Amp_r, Km_r, Tc_r). The recipient strain, *E. coli* C600 (Str_r), exhibits chromosomal resistance to streptomycin. All antibiotics used in this study were sourced from Shanghai Macklin Biochemical Technology Co., Ltd. Detailed strain cultivation procedures are described in Text S1 of the Supporting Information (SI). Analytically pure nanoparticles of WO_3, WS_2, SnO_2, SnS_2, CuO, CuS, ZnO, and ZnS (purity > 99.0%) with similar particle sizes were obtained from Shanghai Macklin Biochemical Technology Co., Ltd. The detailed particle sizes and Zeta potential characteristics of these nanoparticles are provided in Table S1. The selected nanoparticle types have been detected in aquatic environments and represent the major ENPs used in various fields. For instance, ZnO and CuO serve as antibacterial agents in medicine [22], SnO_2 functions in sensors, solar cells, and batteries [23], while CuS, ZnS, and SnS_2 are used in electrochemical devices and electrocatalysis [17,24].

2.2. Conjugation experiments

Donor and recipient bacterial cells, each at a concentration of 10^8 CFU/mL, were mixed at a 1:1 ratio in PBS buffer (pH = 7.2) to establish a conjugative mating system. Based on preliminary conjugation assays conducted in the absence of ENPs, an optimal conjugation period of 8 h was determined (Fig. S1). ENPs were introduced into the mixture at concentrations of 0, 0.01, 0.1, 1, 10, and 100 mg/L, reflecting both environmentally relevant levels (0.01 and 0.1 mg/L) and elevated pollution scenarios (1–100 mg/L), according to environmentally relevant concentrations of ENPs (Table S2). It should be noted that not all the ENPs had field monitoring data, and the environmentally relevant

concentrations of WO_3, WS_2, SnO_2 and SnS_2 were assumed to be comparable with other ENPs. After 8 h of incubation at 37 °C, the cultures were plated onto Luria-Bertani agar selection plates. Transconjugants were selected using plates supplemented with four antibiotics: 20 mg/L tetracycline, 100 mg/L ampicillin, 33 mg/L kanamycin, and 500 mg/L streptomycin. Recipient strains were selected on plates containing 500 mg/L streptomycin. The conjugative transfer frequency was calculated using Eq. (1)[25].

$$\text{Conjugate transfer frequency} = \frac{\text{Transconjugant cell (CFU/mL)}}{\text{Recipient cell (CFU/mL)}} \quad (1)$$

Conjugation experiments involving other types of nanoparticles were conducted following the same protocol. Additionally, 100 μM thiourea (a ROS scavenger) and 75 μM rotenone (an energy metabolism inhibitor) were added to the conjugation system to investigate the effects of ROS and ATP on conjugative transfer. The successful transfer of the RP4 plasmid was further confirmed through gel electrophoresis, as detailed in Text S2 and Table S3. All experiments were carried out with biological triplicates. Prior to the conjugation assays, the minimum inhibitory concentrations (MIC) of the selected ENPs were determined according to standard methods [26] and the results are shown in Table S4, which indicates no bacterial growth inhibition at the tested concentrations of ENPs.

2.3. Molecular dynamics simulations

1,2-Dipalmitoyl-sn-glycero-3-phosphatidylcholine (DPPC) was used as a model membrane lipid, and its bilayer structure was built using the CHARMM-GUI server [27]. The crystal structures of WO_3 and WS_2 were obtained based on their X-ray diffraction (XRD) lattice parameters (Fig. S2), and molecular models with dimensions of approximately 1–2 nm were constructed. The simulations applied the FF14SB force field for proteins, the General Amber Force Field (GAFF) for small molecules, and the TIP3P model for water molecules. All molecular dynamics simulations were conducted using GROMACS (version 2021) [28]. Additional simulation details are provided in Text S3.

2.4. RNA sequencing and transcriptomic analysis

RNA sequencing (RNA-seq) was performed on cultures treated with WO_3 and WS_2 NPs at two distinct concentrations: 0.1 mg/L, which exhibited the strongest promotion of conjugative transfer, and 100 mg/L, which showed an inhibitory effect. Gene expression levels and associated metabolic pathways were analyzed using a suite of bioinformatic tools and databases, including DESeq2 (version 1.12.4), RSEM, Kyoto encyclopedia of genes and genomes (KEGG), and Gene Ontology (GO) databases. Transcript abundance was quantified in Transcripts Per Million (TPM). Differentially expressed genes (DEGs) between the control and NPs-treated groups were identified based on the thresholds of $|\log_2(\text{fold change})| > 2$, $P < 0.05$. All RNA extraction and sequencing procedures were performed by Majorbio Gene Technology Co., Ltd. (Shanghai, China). Detailed information on bioinformatic analysis is described in Text S4.

2.5. Other analytical methods

Bacterial surface hydrophobicity was determined according to a previously reported method [29]. Cell membrane permeability was evaluated by measuring fluorescence intensity following propidium iodide (PI) staining, while bacterial microstructure was examined through transmission electron microscopy (TEM) as described in Text S5. The zeta potential of cell suspensions was determined using a Zetasizer Nano ZS 90 instrument (Malvern, UK). Intracellular ROS levels were detected with a Cellular ROS Detection Kit (S0033, Beyotime), and intracellular ATP content was quantified using an Enhanced ATP Detection Kit (S0027, Beyotime). For protein analysis, cellular proteins were extracted with a Bacterial Protein Extraction Kit (C600596, Biotech) and quantified with an Enhanced Protein Assay Kit (C503041, Biotech). Polysaccharide content was determined via the phenol-sulfuric acid method using glucose as the standard. The NAD^+/NADH ratio was quantified using the NAD^+/NADH Assay Kit with WST-8 (S0175, Beyotime). Additional detailed procedures for these analytical methods are provided in Text S6.

2.6. Statistical analysis

All data are presented as mean ± standard deviation (S.D.) from biological triplicates. SPSS Statistics 26.0 (IBM, Armonk, NY) was used to perform statistical analyses. One-way analysis of variance (ANOVA) was used for comparisons across multiple groups. Where a significant overall effect was observed, Duncan's post hoc test was applied for further pairwise comparisons. Direct comparisons between two groups were performed using independent-samples t-tests. The significance levels for all statistical tests were set as $^*P < 0.05$, $^{**}P < 0.01$, and $^{***}P < 0.001$. For the ANOVA post hoc results, differences are indicated by letter-based notation, where different letters represent statistically significant differences at $P < 0.05$.

3. Results and discussion

3.1. WO_3 NPs exhibited higher conjugative transfer frequencies than WS_2 NPs

The conjugative transfer frequency was investigated under varying concentrations of WO_3 and WS_2 NPs (Fig. 1a). Compared to the control, a significant increase in conjugative transfer frequency was observed at 0.01 mg/L and 0.1 mg/L for both WO_3 NPs and WS_2 NPs ($P < 0.05$). However, as the concentrations of WO_3 and WS_2 NPs increased to higher pollution levels (1, 10, and 100 mg/L), the fold change in conjugative transfer frequency decreased gradually. No obvious bacterial inactivation was found at the concentration of 100 mg/L (Fig. S3), suggesting the decrease of conjugative transfer frequency at high concentration was not attributable to reduction in donor and recipient cell counts. These results demonstrate that both types of NPs promote conjugative transfer at environmentally relevant concentrations but inhibit it at elevated pollution concentrations. As a comparison, WO_3 NPs promoted the transfer frequency by up to 2.75-fold in comparison to the control (0 mg/L), while WS_2 NPs only increased it by 1.83-fold. In addition, gel electrophoresis of donor, recipient, and transconjugant cells demonstrated that the RP4 plasmid was successfully transferred (Fig. S4). The WO_3-treated group had significantly higher conjugative transfer frequency than the WS_2-treated group ($P < 0.05$), suggesting that WO_3 NPs present a higher risk for ARG transmission under the same concentration. Previously, nano-hematite [30] and CuO NPs [13] were reported to increase conjugative transfer by 1.83- to 2-fold at concentrations ranging from 0.08 to 1 mg/L. In contrast, WO_3 NPs in this study induced a 2.75-fold increase at only 0.1 mg/L. This indicates that WO_3 NPs exert a more pronounced promoting effect than other reported ENPs, underscoring their non-negligible environmental risks. Based on the observed dose-response effects, subsequent mechanistic investigations focused on two representative concentrations-0.1 mg/L (the concentration with the strongest promotion effect) and 100 mg/L (the concentration showing significant inhibition)-to elucidate how WO_3 and WS_2 NPs regulate horizontal gene transfer and to determine why WO_3 NPs exhibit a stronger effect than WS_2 NPs.

3.2. WO_3 NPs induced higher intracellular ROS and ATP levels than WS_2 NPs

Intracellular ROS is a key factor influencing plasmid-mediated conjugative transfer of ARGs [31]. Therefore, the effects of WO_3 and WS_2 NPs on ROS generation were investigated. Both WO_3 and WS_2 NPs

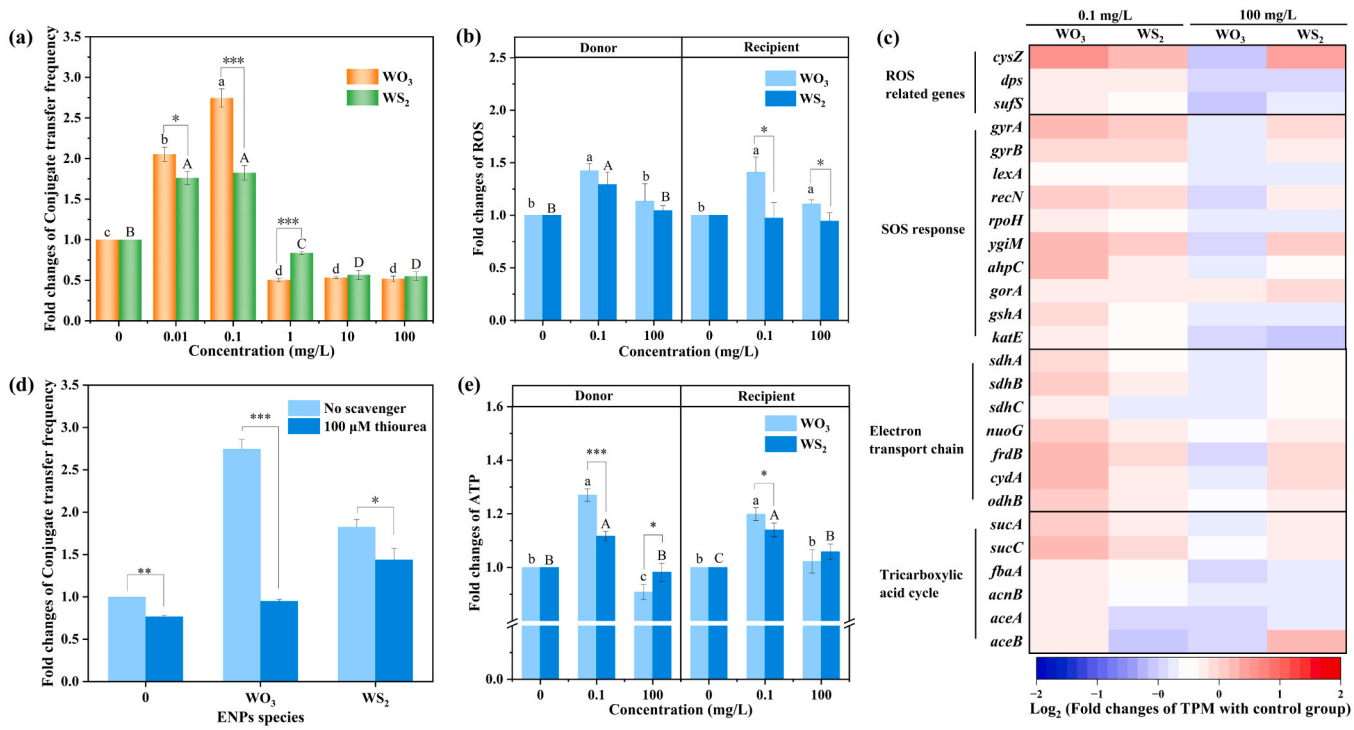

Fig. 1. (a) Conjugative transfer frequency under exposure to WO_3 or WS_2 NPs; (b) Intracellular ROS generation in donor and recipient strains under WO_3 or WS_2 NPs exposure; (c) Gene expression related to ROS response and ATP metabolism under WO_3 or WS_2 NP treatment, presented as log_2 (fold change); (d) Effect of the ROS scavenger (thiourea) on conjugative transfer frequency under exposure to WO_3 or WS_2 NPs; (e) Intracellular ATP levels in bacteria exposed to WO_3 or WS_2 NPs. Significant differences relative to the control group are marked with lowercase letters for WO_3 NPs and uppercase letters for WS_2 NPs (ANOVA, different letters indicate $P < 0.05$). Significant differences between groups treated with and without ROS scavenger, as well as among WO_3 and WS_2 NPs treatment groups, were determined using independent samples *t*-tests (* $P < 0.05$, ** $P < 0.01$, *** $P < 0.001$).

significantly enhanced intracellular ROS levels at 0.1 mg/L, whereas a decline was observed at 100 mg/L ($P < 0.05$), indicating a concentration-dependent response (Fig. 1b). Transcriptome sequencing analysis indicated that exposure to 0.1 mg/L of WO_3 and WS_2 NPs led to significant upregulation of ROS-related genes (*cysZ, dps, sufS*) and SOS pathway genes (*gyrA, gyrB, recN, ygiM, ahpC*) ($P < 0.05$) (Fig. 1c). In contrast, at 100 mg/L, the downregulation of antioxidant enzyme genes (*ahpC*, *sodB, gor*) indicates an alleviation of intracellular oxidative stress under high-concentration conditions. These results suggest that varying concentrations of WO_3 and WS_2 NPs induce differential oxidative stress, aligning with the observed trends in conjugation frequency. To further verify the role of ROS in the enhanced conjugative transfer at 0.1 mg/L WO_3 or WS_2 NPs, the ROS scavenger thiourea was added to the conjugation system. No bacterial inactivation was found with the addition of thiourea scavenger, suggesting negligible effects to donor and recipient cells (Fig. S5). In the WO_3-treated group, conjugative transfer frequency decreased from 2.75-fold to 0.95-fold after scavenger addition (Fig. 1d), confirming the important role of ROS in WO_3-facilitated ARGs transmission. In contrast, the transfer frequency in the WS_2-treated group showed only a modest reduction, from 1.83-fold to 1.44-fold, similar to previous reports that WS_2 NPs cause comparatively small intracellular ROS production [20]. Integrated with transcriptomic analysis (Fig. 1c), WO_3 NPs markedly upregulated genes involved in ROS metabolism (*cysZ, dps, sufS*; up to 1.82-fold), the SOS response pathway (*gyrA, gyrB, recN*), and antioxidant enzymes (*ahpC, katE*), confirming SOS pathway activation. Although WS_2 NPs induced a milder upregulation of ROS-related genes (only up to 1.48-fold), they still activated the SOS response, potentially as a result of their nanoscale characteristics [20].

The ATP level is a crucial regulatory factor for DNA transfer because conjugative transfer requires a lot of energy [32]. In both donor and recipient strains, 0.1 mg/L of the WO_3 and WS_2 NPs significantly increased intracellular ATP ($P < 0.05$), whereas ATP levels decreased at the higher concentration of 100 mg/L (Fig. 1e). ATP is mainly generated via the tricarboxylic acid (TCA) cycle and the electron transport chain (ETC) [33]. The addition of rotenone significantly suppressed conjugative transfer frequency in both 0.1 mg/L WO_3 and WS_2 NPs systems (Fig. S6a), directly demonstrating that ETC activity was necessary for the nanoparticle-promoted conjugation process. Concurrently, while ATP levels declined (Fig. S6b), ROS levels increased markedly (Fig. S6c) with the addition of rotenone, suggesting a bidirectional and threshold-dependent interplay between ROS and ATP in regulating conjugative transfer. The ETC comprises transmembrane complexes I–IV and electron carriers such as ubiquinone and cytochrome C (Fig. S7). Genes related to Complex I (*nuoG*), Complex II (*sdhA, sdhB, frdB*), and Complex IV (*cydA*) were upregulated at 0.1 mg/L WO_3 NP exposure, whereas they were suppressed at 100 mg/L (Fig. 1c). This upregulation indicates enhanced electron and proton flux through the ETC, which stimulates oxygen consumption and ATP synthesis. Conversely, TCA cycle (*aceA*, *aceB*, *acnB*) and ETC (*sdhA*, *sdhB*, *sdhC*) gene downregulation at elevated pollution concentrations likely impaired ETC function and energy supply, inhibiting conjugative transfer. The TCA cycle generates nicotinamide adenine dinucleotide (NADH), which is subsequently utilized via proton motive force (PMF) and the ETC for ATP synthesis. The measured NAD^+/NADH ratio exhibited consistent patterns with gene expression (Fig. S6d), directly validating Complex I's regulatory role in energy metabolism. Notably, although both WO_3 and WS_2 NPs at 0.1 mg/L enhanced conjugative transfer by elevating ATP, their effects differed in magnitude. WO_3 NPs elevated ATP levels to 1.27-fold in donors and 1.20-fold in recipients, whereas WS_2 NPs induced more modest increases of 1.12-fold and 1.14-fold, respectively (Fig. 1e, Fig. S8). Correspondingly, WO_3 NPs significantly upregulated TCA cycle genes (*sucA, sucC, fbaA*) and the ETC genes (*sdhB, nuoG, frdB, cydA*) by 1.11- to 1.55-fold, while WS_2 NPs induced a more moderate upregulation (1.07- to 1.27-fold; $P < 0.05$). Given that the ETC regulates

energy metabolism and bacterial cellular processes [34], and nanoparticle-induced changes in conjugative transfer are closely linked to ETC gene expression [35], the stronger upregulation of ETC genes and higher ATP levels under WO_3 exposure likely improved stress resistance and supplied more energy for plasmid transfer [36]. In contrast, the limited ATP elevation under WS_2 NPs exposure provided only modest energy support, resulting in a lower conjugative transfer frequency compared to the WO_3-treated group.

3.3. WO_3 NPs induced greater cell membrane disruption than WS_2 NPs

Prior research has established a close association between changes in cell membrane permeability and conjugative transfer of ARGs [37]. Thus, the impact of varying concentrations of WO_3 and WS_2 NPs on membrane permeability was evaluated using a PI fluorescence assay. Compared to controls, exposure to 0.01 mg/L WO_3 and WS_2 NPs significantly increased membrane permeability. Specifically, WO_3 NPs increased permeability by 2.13-fold in donors and 1.20-fold in recipients, while WS_2 NPs caused increases of 1.69-fold and 1.19-fold, respectively ($P < 0.05$). In contrast, treatment with 100 mg/L WO_3 and WS_2 NPs reduced membrane permeability (Fig. 2a, Fig. S9). Consistent with these phenotypic observations, the expression levels of genes encoding membrane proteins and permeability (*ompC, ompF, ompR, ompX, osmB, yccA, pal, slyB*) closely correlated with the observed trends (Fig. 2b). Combined with the oxidative stress responses described in Section 3.1, these results indicate that both WO_3 and WS_2 NPs at 0.1 mg/L increase membrane permeability by generating cellular lipid peroxidation and bacterial oxidative stress, thereby facilitating plasmid transfer. However, as the concentration increases, interparticle collisions intensify, promoting the formation of larger aggregates that can attenuate their intrinsic nanoscale effects [30,38]. Consequently, changes in membrane permeability are reduced at 100 mg/L, which aligns with the observed decrease in bacterial conjugative transfer frequency.

The effects of WO_3 and WS_2 NPs on membrane permeability were compared. As shown in Fig. 2a, the fluorescence intensity of the donor strain increased by 2.13-fold ($P < 0.05$) in the WO_3-treated group compared to the control, which is significantly higher than the 1.69-fold increase observed in the WS_2-treated group. TEM images of bacterial cells showed that, in the absence of nanoparticles, bacterial membranes remained smooth and intact with no visible cytoplasmic disruption (Fig. 2c), while WS_2 NPs exposure produced noticeable membrane damage and mild cell adhesion (Fig. 2d). In comparison, WO_3 NPs at the same concentration caused more serious structural alterations, like cytoplasmic leakage and blurred cell boundaries, accompanied by more pronounced cell adhesion (Fig. 2e). These morphological findings confirm that WO_3 NPs induce greater impact on membrane permeability than WS_2 NPs. Gene expression analysis further supported these observations. Treatment with 0.1 mg/L WO_3 NPs significantly upregulated several outer membrane protein-related genes (*creD, ompC, ompT, rbsA, ydiY*) and permeability-associated genes (*dctA, osmB*), with expression increases of up to 3.82-fold (Fig. 2b). Under WS_2 NP exposure, the maximum upregulation of these genes was 2.72-fold ($P < 0.05$). The elevated expression of outer membrane proteins was associated with promoted transmembrane DNA transport [39], and the disruption of lipid bilayer could create additional channels for genetic exchange

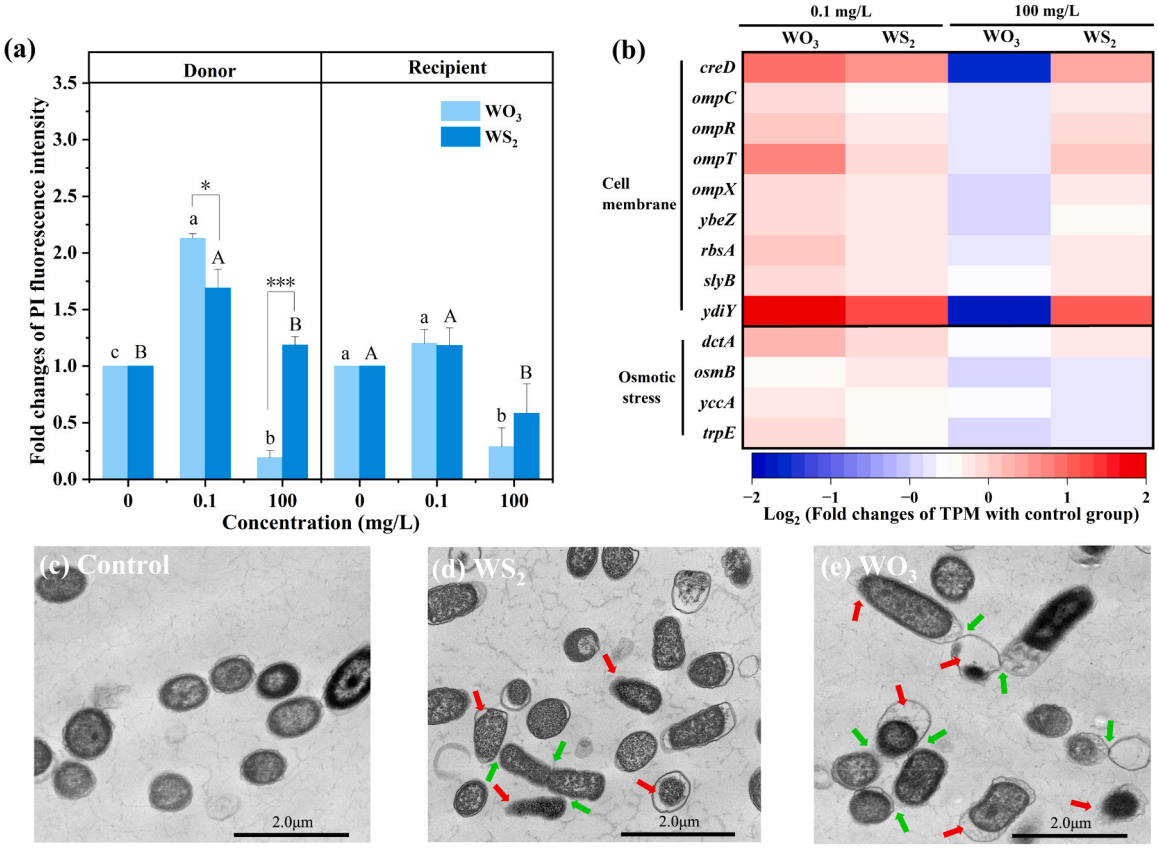

Fig. 2. (a) Fold changes of PI fluorescence intensity corresponding to different dosage of WO_3 and WS_2 NPs respectively; (b) Expression levels of genes associated with membrane integrity and permeability in the conjugation system, presented as $\log_2$ (fold change); TEM images of the conjugation system in the (c) control group, (d) 0.1 mg/L WS_2 NPs treatment group, and (e) 0.1 mg/L WO_3 NPs treatment group. Red arrows indicate cytoplasmic leakage and membrane damage, and green arrows indicate cell-cell contacts. Significant differences relative to the control group are marked with lowercase letters for WO_3 and uppercase letters for WS_2 (ANOVA, different letters indicate $P < 0.05$). Differences between nanoparticle treatments were evaluated using independent samples *t*-test (* $P < 0.05$, *** $P < 0.001$).

between bacteria [40]. Therefore, the stronger membrane disruption and associated upregulation of outer membrane proteins induced by WO_3 NPs correlated with its higher conjugative transfer frequency compared to WS_2 NPs.

3.4. Molecular dynamics simulation confirmed divergent interaction between WO_3/WS_2 molecules with the cell membrane

To gain deep insights into the molecular interaction mechanisms between ENPs and the cell membrane, molecular dynamics simulations were performed. Representative configuration snapshots revealed that both WO_3 and WS_2 molecules remained localized in the aqueous phase without penetrating the DPPC lipid bilayer (Fig. 3a). Density distributions analysis indicates that WO_3 exhibited density peaks closer to the center of the DPPC bilayer (x = 0) compared to WS_2, indicating more intimate contact with the cell membrane (Fig. 3b). Further study of interaction energy revealed that although both nanoparticles associated with the lipid bilayer through van der Waals and electrostatic interactions, the binding of WO_3 engaged primarily via electrostatic forces with an interaction energy of −81.6 kJ/mol, whereas WS_2 was dominated by van der Waals interactions, exhibiting a lower interaction energy of −29.1 kJ/mol (Fig. 3c). This significant energy difference indicates that WO_3 binds more strongly to the lipid bilayer, enabling it to integrate more deeply into the membrane structure.

The Mean square displacement (MSD) of the DPPC-WO_3 system was significantly lower than that of the WS_2 system (Fig. 3d). This finding suggests that WO_3 more effectively restricts lipid lateral diffusion than WS_2, because MSD reflects molecular mobility and is positively correlated with lipid lateral diffusion [41]. The WO_3-DPPC system had lower principles than WS_2-DPPC, according to the effects of the root mean square deviation (RMSD) research (Fig. 3e). As RMSD quantifies structural stability over time, with lower values indicating reduced conformational fluctuations [42], this finding implies that WO_3 enhances membrane structural stability than WS_2. Furthermore, the WO_3-DPPC system's deuterium order parameter (Scd) for the sn-1 lipid chains was significantly lower than in WS_2-DPPC (Fig. 3f). Reduced values indicate a higher lipid tail disorder because Scd reflects the hydrocarbon chain's orientational order [43]. In contrast, the solvent-accessible surface area (SASA) was 637.3 nm^2 for WO_3-DPPC and 634.7 nm^2 for WS_2-DPPC, suggesting that there is no significant difference in membrane porosity between the two systems (Fig. 3g). Overall, WO_3 achieved deeper membrane integration through stronger interactive forces with lipid membranes than WS_2. The stronger interaction by WO_3 not only increased membrane permeability, but also intensified intracellular oxidative stress through amplified membrane disruption, establishing more favorable conditions for the transmembrane transport of plasmid DNA.

3.5. WO_3 NPs promoted intercellular contact between donor and recipient than WS_2 NPs

Intercellular contact is required for plasmid transmission in HGT. By facilitating cell adhesion and aggregation, EPS plays a significant role in promoting this process [44]. Polysaccharides (PS) and proteins (PN) make up the majority of EPS [45]. As shown in Fig. 4a, exposure to 0.1 mg/L WO_3 and WS_2 NPs significantly increased EPS production in both donor and recipient strains ($P < 0.05$), thereby enhancing intercellular contact. In contrast, at 100 mg/L, EPS of recipient cells content significantly decreased, consistent with the downregulation of lipopolysaccharide (LPS) biosynthesis genes (*lpxD, wzzB*). Importantly, the EPS content in the recipient cells increased by 2.90-fold with 0.1 mg/L WO_3 NPs, beating the 2.48-fold improvement brought on by WS_2 NPs. Further, transcriptomic analysis revealed that WO_3 NPs caused a 2.13-fold upregulation of genes involved in protein transport (*secD,*

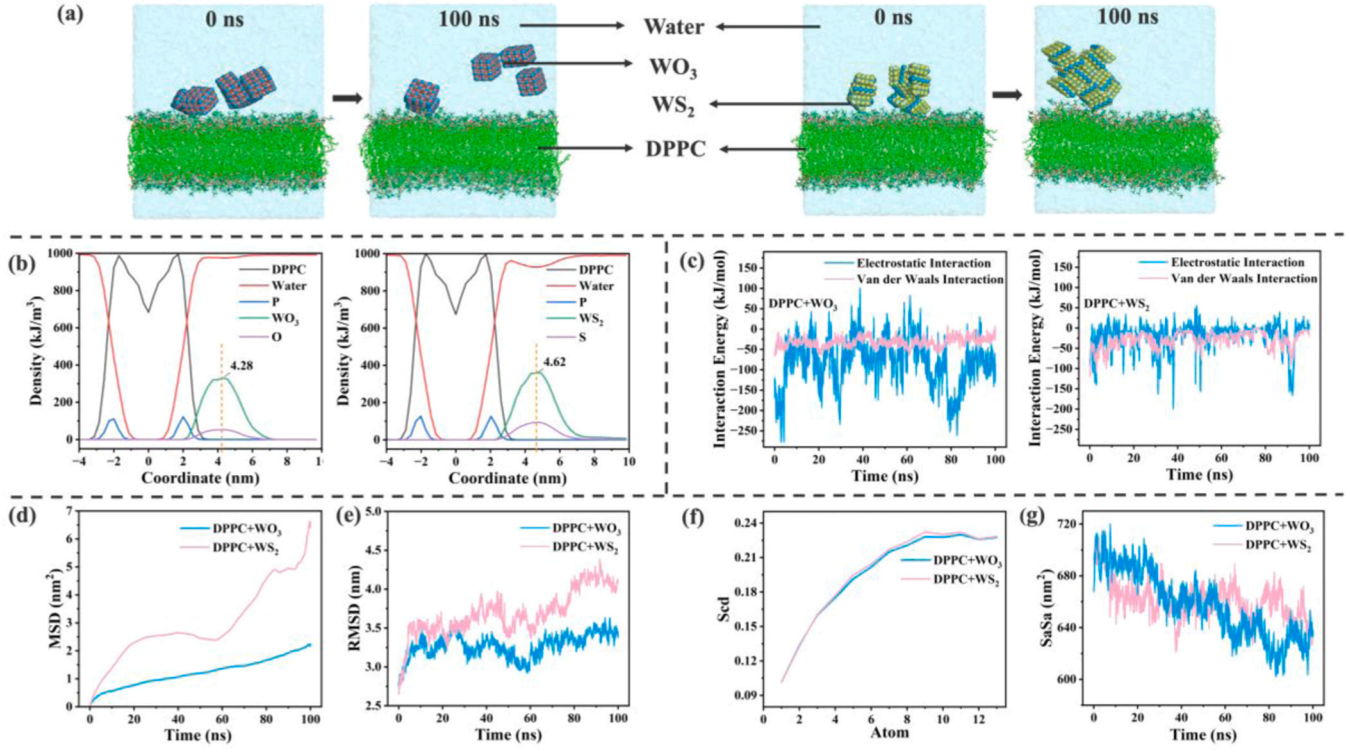

Fig. 3. (a) Configuration snapshots at 0 and 100 ns obtained from simulations of different molecular materials and DPPC bilayers. Red-blue molecules represent WO_3 molecules, yellow-blue molecules represent WS_2 molecules, light blue represents water molecules, and green represents the DPPC bilayer; (b) Density distributions of each component, (c) energy contribution components, and (d) mean square displacement (MSD) profiles for DPPC-WO_3 and DPPC-WS_2 systems; (e) Root mean square deviation (RMSD), (f) deuteration order parameter for sn^{-1} chain (Scd), and (g) Solvent-accessible surface area (SaSa) of DPPC- WO_3 and DPPC-WS_2 complexes.

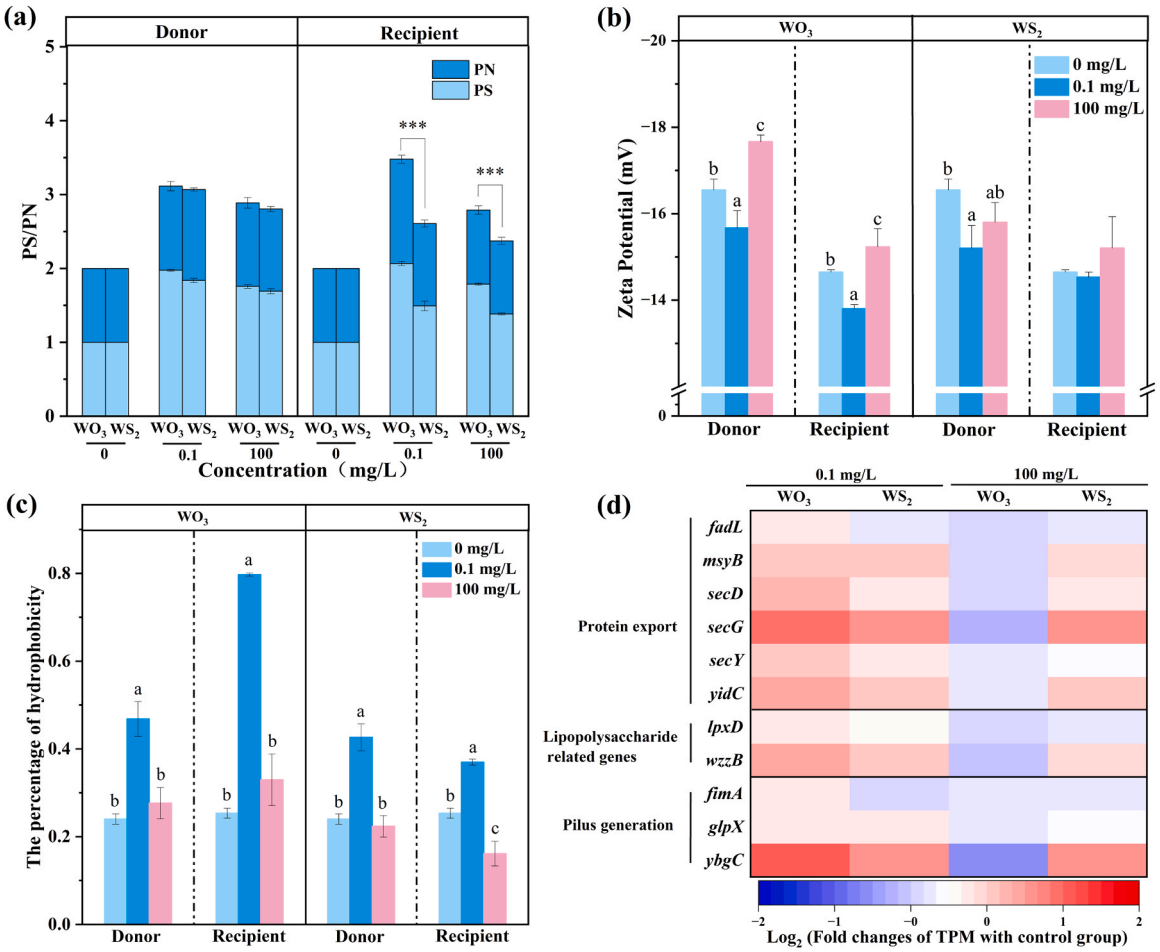

Fig. 4. (a) Changes in the PS/PN of bacterial strains under exposure to WO_3 or WS_2 NPs; (b) Zeta potential and (c)the percentage of hydrophobicity of strains after treatment with WO_3 or WS_2 NPs; (d) Significantly differentially expressed genes related to protein transport, lipopolysaccharide synthesis, and bacterial motility in conjugation systems under WO_3 or WS_2 NP exposure, shown as $\log_2$ (fold change). Lowercase letters denote significant differences between the exposure groups and the control group (ANOVA, $P < 0.05$). Significant differences between WO_3 and WS_2 NPs treatments were determined by independent samples *t*-tests (*** $P < 0.001$).

secG, secY, yidC) and LPS biosynthesis genes (*lpxD, wzzB*), as opposed to a 1.87-fold increase under WS_2 NPs exposure (Fig. 4d). The Sec secretion system, which mediates protein translocation across the membrane, serves as a major pathway for extracellular protein export [46], while *lpxD* encodes an LPS synthase and *wzzB* regulates O-antigen chain length [47]. The coordinated upregulation of these genes supports enhanced EPS content. These results demonstrate that WO_3 NPs have a stronger regulatory effect on genes involved in LPS production and protein transport, making EPS production more marked than WS_2 NPs.

To determine the adjustments to bacterial adhesion, the zeta potential and hydrophobicity of the donor and recipient were further examined, as depicted in Fig. 4b. Compared to the controls, WO_3 and WS_2 NPs at 0.1 mg/L significantly reduced the surface charge of the bacterial suspensions ($P < 0.05$). A less negative surface charge reduces electrostatic repulsion between cells, thereby promoting cell adhesion [29]. At 100 mg/L, the zeta potential rebounded, best possible as a result of nanoparticle deposition forming a coating layer on cell surfaces (Fig. 4b). Notably, WO_3 NPs at 0.1 mg/L reduced the zeta potential of recipient cells from −14.65 mV to −13.8 mV, while WS_2 NPs caused a smaller reduction to −14.5 mV. Bacterial surface hydrophobicity, which has a strong correlation with adhesion capacity, was also examined [48]. Both types of NPs at 0.1 mg/L significantly enhanced hydrophobicity compared with the controls ($P < 0.05$), while hydrophobicity decreased at 100 mg/L treatments (Fig. 4c). Specifically, 0.1 mg/L WO_3 NPs increased the donor and recipient strains' hydrophobicity by 1.95-fold and 3.15-fold compared with the controls, respectively, while WS_2 NPs caused smaller increases of 1.77-fold and 1.46-fold. As shown in Fig. 4d, gene expression analysis further revealed that exposure to 0.1 mg/L WO_3 NPs led to a 1.76-fold upregulation of flagellar motility-related genes (*glpX, ybgC*). Flagella, driven by proton motive force, influence cell motility and intercellular contact. In contrast, these genes were merely upregulated 1.48-fold by WS_2 NPs, suggesting relatively limited enhancement of motility and interbacterial proximity. These results indicate that WO_3 NPs are more effective at promoting bacterial contact and conjugative transfer than WS_2 NPs by exerting stronger effects on zeta potential reduction, hydrophobicity enhancement, and upregulation of flagellar motility-related genes.

3.6. Comparative analysis of the differential mechanisms of WO_3 and WS_2 NPs

WO_3 and WS_2 NPs, according to this research, significantly promoted the transfer of ARGs at environmentally relevant concentrations, whereas elevated concentrations inhibited this process. This concentration-dependent behavior was brought on by matching variations in cellular functional states and their associated gene regulatory networks, which were upregulated at environmentally relevant concentrations and downregulated at elevated pollution concentrations. Specifically, WO_3 and WS_2 facilitated ARGs transfer at concentrations of 0.1 mg/L through increased membrane permeability, elevated ATP

levels, and enhanced cell adhesion, while this promotion effect was attenuated at high concentrations (100 mg/L) due to downregulation of membrane protein genes, decreased ATP generation, and reduced cell adhesion. Although both WO_3 and WS_2 increased conjugative transfer at environmentally relevant concentrations, WO_3 NPs produced a higher conjugation frequency than WS_2 NPs. The following multi-level synergistic mechanisms are responsible for this differential promotion (Fig. 5). Firstly, WO_3 NP exposure induces significantly higher intracellular ROS levels, stronger expression of ROS-related genes, and a more pronounced SOS response than WS_2 NPs, as evidenced in Fig. 1b. Elevated ROS and SOS activity promote lipid peroxidation, thereby disrupting the lipid bilayer and facilitating intercellular communication, which accelerates ARGs transfer. Secondly, molecular dynamics simulations confirmed that WO_3 establishes deeper contact with the DPPC bilayer through stronger interaction energy, while concurrently reducing lipid fluidity and increasing membrane disorder (Fig. 3). These molecular-level insights reveal why WO_3 NPs affect membrane permeability more pronouncedly than WS_2 NPs. Thirdly, as conjugative transfer is a highly energy-intensive process, the ETC is key to bacterial energy production, growth, and communication [34]. Compared to WS_2 NPs, contact with WO_3 NPs resulted in higher intracellular ATP levels and a stronger upregulation of ETC-related genes (Fig. 1c and e), thereby supplying more energy to drive conjugative transfer. Cellular interaction properties were further examined because conjugative HGT requires strong intercellular contact [33]. WO_3 NPs significantly increased the PN/PS content in bacterial EPS, enhanced cell adhesion capacity, and upregulated genes involved in protein transport, lipopolysaccharide synthesis, and flagellar motility relative to WS_2 NPs (Fig. 4). In addition, KEGG enrichment analysis indicated that WO_3 NPs and WS_2 NPs mainly affect pathways involved in cellular metabolism, environmental information processing, and genetic information processing (Fig. S10, S11). Under WO_3 NPs exposure, signal transduction and membrane transport pathways were significantly enriched, and the upregulation of related genes implies an enhanced potential for exogenous DNA uptake and integration. Furthermore, compared to WS_2, WO_3 NPs induced stronger enrichment in key metabolic pathways, including energy, carbohydrate, and amino acid metabolism, suggesting that bacteria under WO_3 NPs stress maintain more active energy and biosynthetic activities, which may provide a physiological basis favoring horizontal gene transfer. Collectively, WO_3 NPs influenced a wider spectrum of functional categories, spanning resistance associated regulation and transport systems as well as core metabolic processes. These findings demonstrate that WO_3 NPs exert a broader and more integrated effect on bacterial gene expression than WS_2 NPs, corresponding to a higher potential risk of promoting the horizontal dissemination of ARGs. Finally, this difference may be related to the higher electronegativity of oxygen atom ($\chi = 3.44$) in WO_3 compared to sulfur atom ($\chi = 2.58$) in WS_2, which allows WO_3 to extract electrons from the lipid bilayer more easily, inducing lipid peroxidation and thereby enhancing cell membrane permeability to facilitate plasmid conjugative transfer. In summary, WO_3 NPs promote HGT more effectively than WS_2 NPs through synergistic enhancement of intracellular ROS and the SOS response, increased membrane permeability, elevated energy supply, and facilitation of cell contact, coupled with broader regulation of key metabolic genes.

3.7. *Potential differential roles of MONPs and MSNPs on the conjugative transfer of ARGs*

To explore the differential roles of MONPs and MSNPs in regulating conjugative transfer of ARGs, a systematic comparison was conducted between additional representative MONPs (CuO, ZnO, SnO_2) and their corresponding MSNPs (CuS, ZnS, SnS_2). As shown in Fig. 6, both MONPs and MSNPs enhanced conjugative transfer at environmentally relevant concentrations of 0.01 and 0.1 mg/L (Fig. 6a, b), but exhibited inhibitory effects at elevated pollution concentrations (1–100 mg/L) (Fig. 6c-e). Notably, at 0.01 mg/L, MONPs increased the RP4 plasmid transfer

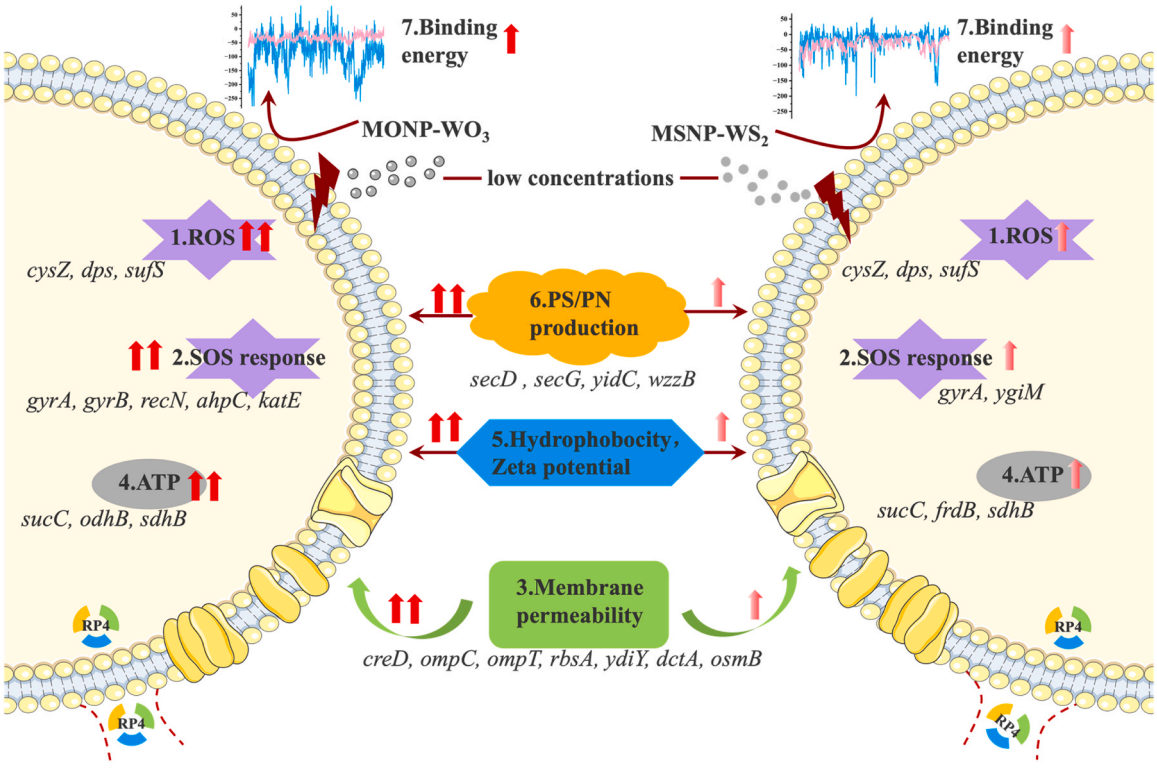

Fig. 5. Mechanism diagram of WO_3 and WS_2 NPs exposure promoting conjugative transfer. Exposure to WO_3 and WS_2 NPs induces elevated levels of (1) ROS and (2) oxidative stress in *E. coli*, leading to (3) cell membrane damage. This damage forms membrane channels that enhance plasmid transfer. (7) The binding energies of WO_3 and WS_2 NPs to the cell membrane, respectively, explain their differential interactions. WO_3 and WS_2 NPs stimulate (4) ATP synthesis, thereby boosting energy supply. Additionally, they alter (5) hydrophobicity, zeta potential, and (6) PN/PS generation, enhancing bacterial contact to facilitate plasmid transfer.

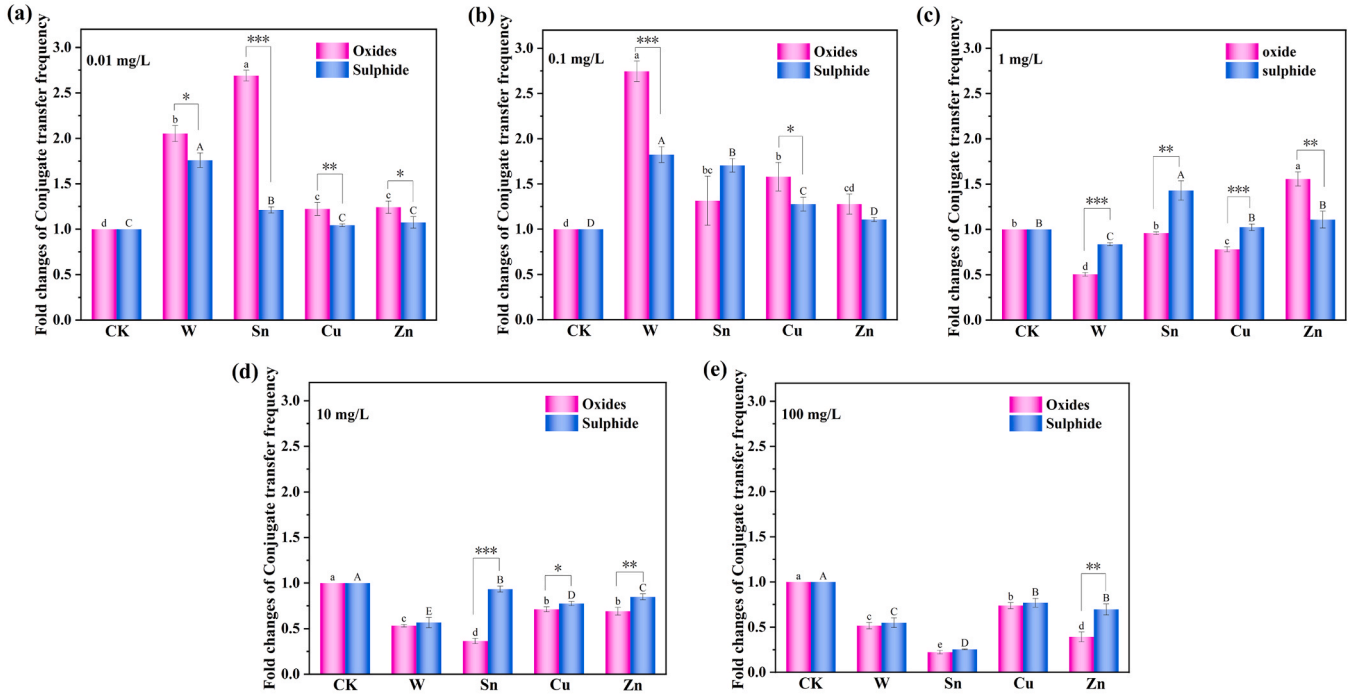

Fig. 6. Fold changes of conjugate transfer frequency upon exposure to MONPs and their corresponding MSNPs at concentrations of (a) 0.01, (b) 0.1, (c) 1, (d) 10, and (e) 100 mg/L. Lowercase letters indicate significant differences between MONPs and the control group (0 mg/L), while uppercase letters denote significant differences between MSNPs and the control group (ANOVA, $P < 0.05$). Significant differences between MONPs and their corresponding MSNPs treatments were determined by independent samples *t*-tests (* $P < 0.05$, ** $P < 0.01$, *** $P < 0.001$).

frequency by 1.06- to 2.7-fold, whereas MSNPs resulted in a 1.04- to 1.76-fold increase, indicating a significantly stronger promotive effect by MONPs (Fig. 6a). These results are consistent with those of WO_3 and WS_2 NPs. Similar to WO_3/WS_2 NPs, the differential effects of MONPs and MSNPs on oxidative stress, cellular functional states, gene regulatory networks, and interaction capacity explain their differing capacities to promote plasmid transfer. In addition, from a chemistry point of view, this divergence may originate from the electronegativity differences of their constituent atoms. The oxygen atoms in MONPs possess higher electronegativity ($\chi = 3.44$) than that of sulfur atoms ($\chi = 2.58$) in MSNPs. The higher electronegativity of oxygen atoms facilitates electron abstraction from cell membrane lipids, leading to lipid oxidation. This is consistent with the experimental observations that WO_3 induces greater membrane permeability enhancement (Fig. 2a), more pronounced membrane structural damage (Fig. 2c-e), and stronger upregulation of membrane lipid-related genes (Fig. 2b) than WS_2. Furthermore, molecular dynamics simulations confirm that WO_3 possesses higher binding affinity to lipid bilayers, offering molecular-level evidence for the electronegativity-driven membrane interaction mechanism. In contrast, the lower electronegativity of sulfur atoms in MSNPs reduces their tendency to initiate peroxidation reactions. Huang et al., [49] reported that sulfide compounds generated through anaerobic treatment can alleviate CuO NP-induced oxidative stress. Similarly, sulfidation of AgNPs to form Ag_2S was found to reduce their microbial toxicity in sewage sludge systems [50], suggesting sulfidation could alleviate membrane peroxidation reactions. Nevertheless, more direct atomic-level evidences of electron transfer are needed to further validate the electronegativity-driven mechanism in future work. Overall, MONPs may pose higher environmental risks than MSNPs due to their stronger promotion of antibiotic resistance dissemination via plasmid-mediated HGT. However, it should be noted that this study has limitations of not exhaustively investigated the impacts of all the MONPs and MSNPs on the ARGs dissemination. Besides electronegativity of anion atom, other material characteristics (e.g. surface functional groups, particle sizes, surface charges) may also affect the regulating ability. Future studies are still needed to decipher the general discrepancy between MONPs and MSNPs, probably by machine learning and artificial intelligence, thus providing better guidance for management of ENPs-induced ARGs propagation in water environments.

4. Conclusions

This study systematically investigated the differential effects of WO_3 and WS_2 NPs on regulating the conjugative transfer frequency of ARGs. Results found that both WO_3 and WS_2 NPs promote conjugative transfer at environmentally relevant concentrations (0.01–0.1 mg/L) but inhibit it at elevated pollution concentrations (1–100 mg/L), while WO_3 NPs induced significantly higher conjugative transfer frequency than WS_2 NPs. Mechanistically, WO_3 NPs induce greater intracellular ROS and ATP production, leading to stronger oxidative stress, increased membrane permeability, and lipid peroxidation compared to WS_2. Molecular dynamics simulations show WO_3 interacts with lipid bilayers more intensely, causing greater disruption to membrane structure and fluidity. Transcriptomic analysis confirmed that WO_3 NPs induced stronger upregulation of genes involved in the SOS response, outer membrane proteins, lipopolysaccharide biosynthesis, and bacterial motility compared to WS_2 NPs. Further verification with other MONPs (CuO, ZnO, SnO_2) and their corresponding MSNPs (CuS, ZnS, SnS_2) consistently demonstrated that MONPs promote conjugative transfer more potently than their sulfide counterparts at environmentally relevant concentrations, suggesting the potential broad applicability of this phenomenon, which may be attributed to the higher electronegativity of oxygen atoms in MONPs than sulfur atoms in MSNPs, enhancing electron extraction capacity and subsequent membrane interactions. These findings not only advance the understanding of ARG dissemination mechanisms under environmental stress but also provide a scientific basis for assessing the public health risks of ENPs and their differential roles in the spread of antibiotic resistance, thereby supporting the safe application and sustainable management of nanotechnology.

Environmental implication

Antibiotic resistance poses a significant threat to human health, yet the distinct effects of MONPs and MSNPs on the transmission of ARGs remain unclear. This study systematically evaluated the factors driving conjugative transfer of ARGs using WO_3 and WS_2 NPs as model nanoparticles. The molecular mechanisms were revealed by combining molecular dynamics simulations and transcriptomic analysis. Importantly, our findings indicated that the tested MONPs present a higher environmental risk than MSNPs in accelerating the dissemination of ARGs. These results offer valuable insights for ecological safety assessments of nanomaterials and for developing targeted strategies to control the spread of ARGs.

CRediT authorship contribution statement

Zongling Tang: Writing – original draft, Investigation, Formal analysis, Data curation. **Chao Wang:** Visualization, Resources. **Wenhai Liu:** Methodology, Formal analysis. **Jialin Shi:** Validation, Investigation. **Fan Wang:** Validation, Software. **Wanjun Wang:** Writing – review & editing, Supervision, Project administration, Funding acquisition, Conceptualization.

Declaration of Competing Interest

The authors declare that they have no known competing financial interests or personal relationships that could have appeared to influence the work reported in this paper.

Acknowledgements

This work was supported by National Natural Science Foundation of China (42377365, 42122056), Guangdong Basic and Applied Basic Research Foundation (2021B1515020063, 2022A1515010815), and National Key Research and Development Program of China (2021YFC1808901).

Appendix A. Supporting information

Supplementary data associated with this article can be found in the online version at doi:10.1016/j.jhazmat.2026.141653.

Data availability

Data will be made available on request.

References

[1] Nazir, A., Nazir, A., Zuhair, V., Aman, S., Sadiq, S.U.R., Hasan, A.H., et al., 2025. The global challenge of antimicrobial resistance: mechanisms, case studies, and mitigation approaches. Health Sci Rep 8, e71077.
[2] Xu, Z., Zhao, D., Lu, J., Liu, J., Dao, G., Chen, B., et al., 2023. Multiple roles of nanomaterials along with their based nanotechnologies in the elimination and dissemination of antibiotic resistance. Chem Eng J 455, 140927.
[3] Zhang, T.T., Fan, L.Y., Zhang, Y.N., 2025. Antibiotic resistance genes in aquatic systems: sources, transmission, and risks. Aquat Toxicol 284, 107392.
[4] Baker, K.S., Dallman, T.J., Field, N., Childs, T., Mitchell, H., Day, M., et al., 2018. Horizontal antimicrobial resistance transfer drives epidemics of multiple Shigella species. Nat Commun 9, 1462.
[5] He, K., Xue, B., Yang, X., Wang, S., Li, C., Zhang, X., et al., 2022. Low-concentration of trichloromethane and dichloroacetonitrile promote the plasmid-mediated horizontal transfer of antibiotic resistance genes. J Hazard Mater 425, 128030.
[6] Wang, Q., Liu, L., Hou, Z.L., Wang, L.T., Ma, D., Yang, G., et al., 2020. Heavy metal copper accelerates the conjugative transfer of antibiotic resistance genes in freshwater microcosms. Sci Total Environ 717, 137055.
[7] Zhang, Y., Gu, A.Z., He, M., Li, D., Chen, J., 2017. Subinhibitory concentrations of disinfectants promote the horizontal transfer of multidrug resistance genes within and across Genera. Environ Sci Technol 51, 570–580.
[8] Lu, J., Yu, Z., Ding, P., Guo, J., 2022. Triclosan promotes conjugative transfer of antibiotic resistance genes to opportunistic pathogens in environmental microbiome. Environ Sci Technol 56, 15108–15119.
[9] Wang, F., Hu, Z., Wang, W., Wang, J., Xiao, Y., Shi, J., et al., 2024. Selective enrichment of high-risk antibiotic resistance genes and priority pathogens in freshwater plastisphere: unique role of biodegradable microplastics. J Hazard Mater 480, 135901.
[10] Sharma, V.K., Filip, J., Zboril, R., Varma, R.S., 2015. Natural inorganic nanoparticles - formation, fate, and toxicity in the environment. Chem Soc Rev 44, 8410–8423.
[11] Qiu, Z., Yu, Y., Chen, Z., Jin, M., Yang, D., Zhao, Z., et al., 2012. Nanoalumina promotes the horizontal transfer of multiresistance genes mediated by plasmids across genera. PNAS 109, 4944–4949.
[12] Wang, X., Yang, F., Zhao, J., Xu, Y., Mao, D., Zhu, X., et al., 2018. Bacterial exposure to ZnO nanoparticles facilitates horizontal transfer of antibiotic resistance genes. Nanoimpact 10, 61–67.
[13] Zhang, S., Wang, Y., Song, H., Lu, J., Yuan, Z., Guo, J., 2019. Copper nanoparticles and copper ions promote horizontal transfer of plasmid-mediated multi-antibiotic resistance genes across bacterial genera. Environ Int 129, 478–487.
[14] Li, G., Chen, X., Yin, H., Wang, W., Wong, P.K., An, T., 2020. Natural sphalerite nanoparticles can accelerate horizontal transfer of plasmid-mediated antibiotic-resistance genes. Environ Int 136, 105497.
[15] Xu, Z., Hu, S., Zhao, D., Xiong, J., Li, C., Ma, Y., et al., 2024. Molybdenum disulfide nanosheets promote the plasmid-mediated conjugative transfer of antibiotic resistance genes. J Environ Manag 358, 120827.
[16] Baig, U., Gondal, M.A., Rehman, S., Akhtar, S., 2020. Facile synthesis, characterization of nano-tungsten trioxide decorated with silver nanoparticles and their antibacterial activity against water-borne gram-negative pathogens. Appl Nanosci 10, 851–860.
[17] Chen, Z., Zhang, R., Wang, T., Peng, Y., Zhou, Q., Cao, P., et al., 2025. Nanosheet-shaped WS2/ICG nanocomposite for photodynamic/ photothermal synergistic bacterial clearance and cutaneous regeneration on infectious wounds. Mat Sci Eng CMater 169, 214192.
[18] Tijani, J.O., Abdullahi, M.N., Bankole, M.T., Mustapha, S., Egbosiuba, T.C., Ndamitso, M.M., et al., 2021. Photocatalytic and toxicity evaluation of local dyeing wastewater by aluminium/boron doped WO3 nanoparticles. J Water Process Eng 44, 102376.
[19] Francis, D.V., Jayakumar, M.N., Ahmad, H., Gokhale, T., 2023. Antimicrobial activity of biogenic metal oxide nanoparticles and their synergistic effect on clinical pathogens. Int J Mol Sci 24, 9998.
[20] Liu, X., Duan, G., Li, W., Zhou, Z., Zhou, R., 2017. Membrane destruction-mediated antibacterial activity of tungsten disulfide (WS2). RSC Adv 7, 37873–37880.
[21] Lu, J., Wang, Y., Jin, M., Yuan, Z., Bond, P., Guo, J., 2020. Both silver ions and silver nanoparticles facilitate the horizontal transfer of plasmid-mediated antibiotic resistance genes. Water Res 169, 115229.
[22] Otinov, G.D., Lokteva, A.V., Petrova, A.D., Zinchenko, I.V., Isaeva, M.V., Kovtunov, E.A., et al., 2020. Positive and negative effects of metal oxide nanoparticles on antibiotic resistance genes transfer. Antibiotics 9, 742.
[23] Nazarov, D.V., Bobrysheva, N.P., Osmolovskaya, O.M., Osmolovsky, M.G., Smirnov, V.M., 2015. Atomic layer deposition of tin dioxide nanofilms: a review. Rev Adv Mater Sci 40, 262–275.
[24] Yan, X., Michael, E., Komarneni, S., Brownson, J.R., Yan, Z.-F., 2013. Microwave- and conventional-hydrothermal synthesis of CuS, SnS and ZnS: Optical properties. Ceram Int 39, 4757–4763.
[25] Li, H., Wang, Q., Wang, Y., Liu, Y., Zhou, J., Wang, T., et al., 2024. EDTA enables to alleviate impacts of metal ions on conjugative transfer of antibiotic resistance genes. Water Res 257, 121659.
[26] Zhang, Y., Pei, M., Zhang, B., He, Y., Zhong, Y., 2021. Changes of antibiotic resistance genes and bacterial communities in the advanced biological wastewater treatment system under low selective pressure of tetracycline. Water Res 207, 117834.
[27] Lee, J., Patel, D.S., Stahle, J., Park, S.J., Kern, N.R., Kim, S., et al., 2019. CHARMM-GUI membrane builder for complex biological membrane simulations with glycolipids and lipoglycans. J Chem Theory Comput 15, 775.
[28] Abraham, M.J., Murtola, T., Schulz, R., Páll, S., Smith, J.C., Hess, B., et al., 2015. GROMACS: high performance molecular simulations through multi-level parallelism from laptops to supercomputers. SoftwareX 1-2, 19–25.
[29] Liao, J., Huang, H., Chen, Y., 2019. CO2 promotes the conjugative transfer of multiresistance genes by facilitating cellular contact and plasmid transfer. Environ Int 129, 333–342.
[30] Wu, S., Ren, P., Wu, Y., Liu, J., Huang, Q., Cai, P., 2022. Effects of hematite on the dissemination of antibiotic resistance in pathogens and underlying mechanisms. J Hazard Mater 431, 128537.
[31] Zhou, Y., Li, J., Wen, X., Li, Q., 2023. Antibiotic resistance gene profiles and evolutions in composting regulated by reactive oxygen species generated via nano ZVI loaded on biochar. Sci Total Environ 902, 166487.
[32] Chen, M.M., Zhang, Y.-Q., Cheng, L.-C., Zhao, F.-J., Wang, P., 2024. Photoaged nanoplastics with multienzyme-like activities significantly shape the horizontal transfer of antibiotic resistance genes. J Hazard Mater 475, 134884.
[33] Yu, K., Chen, F., Yue, L., Luo, Y., Wang, Z., Xing, B., 2020. CeO2 nanoparticles regulate the propagation of antibiotic resistance genes by altering cellular contact and plasmid transfer. Environ Sci Technol 54, 10012–10021.
[34] Jung, H.-M., Han, J.-H., Oh, M.-K., 2021. Improved production of 2,3-butanediol and isobutanol by engineering electron transport chain in Escherichia coli. Microb Biotechnol 14, 213–226.
[35] Huang, H., Liao, J., Zheng, X., Chen, Y., Ren, H., 2019. Low-level free nitrous acid efficiently inhibits the conjugative transfer of antibiotic resistance by altering intracellular ions and disabling transfer apparatus. Water Res 158, 383–391.

[36] Wu, Y., Yan, H., Zhu, X., Liu, C., Chu, C., Zhu, X., et al., 2022. Biochar effectively inhibits the horizontal transfer of antibiotic resistance genes via restraining the energy supply for conjugative plasmid transfer. Environ Sci Technol 56, 12573–12583.
[37] Feng, G., Huang, H., Chen, Y., 2021. Effects of emerging pollutants on the occurrence and transfer of antibiotic resistance genes: a review. J Hazard Mater 420, 126602.
[38] Nguyen, V.T., Pham, N.H., Papavassiliou, D.V., 2024. Prediction of the aggregation rate of nanoparticles in porous media in the diffusion-controlled regime. Sci Rep 14, 1916.
[39] Yan, X.J., Liu, W.W., Wen, S.F., Wang, L.J., Zhu, L.S., Wang, J., et al., 2023. Effect of sulfamethazine on the horizontal transfer of plasmid-mediated antibiotic resistance genes and its mechanism of action. J Environ Sci 127, 399–409.
[40] Ye, T., Li, Y.B., Zhou, X.M., Ye, Y.H., Liu, X.R., Xiong, W.P., 2025. Hormesis-like effects of black phosphorus nanosheets on the spread of multiple antibiotic resistance genes. J Hazard Mater 487, 137207.
[41] Wu, J., Zhou, J.-H., Liu, D.-F., Wu, J., He, R.-L., Cheng, Z.-H., et al., 2023. Phthalates promote dissemination of antibiotic resistance genes: an overlooked environmental risk. Environ Sci Technol 57, 6876–6887.
[42] Hu, X., Waigi, M.G., Yang, B., Gao, Y., 2022. Impact of plastic particles on the horizontal transfer of antibiotic resistance genes to bacterium: dependent on particle sizes and antibiotic resistance gene vector replication capacities. Environ Sci Technol 56, 14948–14959.
[43] Wang, Y., Wang, Q., Zhang, G., Li, Y., Guo, H., Zhou, J., et al., 2024. Masks as a new hotspot for antibiotic resistance gene spread: reveal the contribution of atmospheric pollutants and potential risks. Environ Sci Technol 58, 16100–16111.
[44] Wang, H., Xu, K., Wang, J., Feng, C., Chen, Y., Shi, J., et al., 2023. Microplastic biofilm: an important microniche that may accelerate the spread of antibiotic resistance genes via natural transformation. J Hazard Mater 459, 132085.
[45] More, T.T., Yadav, J.S.S., Yan, S., Tyagi, R.D., Surampalli, R.Y., 2014. Extracellular polymeric substances of bacteria and their potential environmental applications. J Environ Manag 144, 1–25.
[46] Tsirigotaki, A., De Geyter, J., Sostaric, N., Economou, A., Karamanou, S., 2017. Protein export through the bacterial Sec pathway. Nat Rev Microbiol 15, 21–36.
[47] Ranjith, P.K., Mary, Y.S., Panicker, C.Y., Anto, P.L., Armakovic, S., Armakovic, S.J., et al., 2017. New quinolone derivative: spectroscopic characterization and reactivity study by DFT and MD approaches. J Mol Struct 1135, 1–14.
[48] Shi, H., Hu, X., Xu, J., Hu, B., Ma, L., Lou, L., 2023. Conjugation-mediated transfer of antibiotic resistance genes influenced by primary soil components and underlying mechanisms. Sci Total Environ 865, 161232.
[49] Huang, H., Zheng, X., Yang, S., Chen, Y., 2019. More than sulfidation: roles of biogenic sulfide in attenuating the impacts of CuO nanoparticle on antibiotic resistance genes during sludge anaerobic digestion. Water Res 158, 1–10.
[50] Courtois, P., Rorat, A., Lemiere, S., Guyoneaud, R., Attard, E., Levard, C., et al., 2019. Ecotoxicology of silver nanoparticles and their derivatives introduced in soil with or without sewage sludge: a review of effects on microorganisms, plants and animals. Environ Pollut 253, 578–598.